HHS Public Access

Author manuscript

NMR Biomed. Author manuscript; available in PMC 2016 November 01.

Published in final edited form as:

NMR Biomed. 2015 November ; 28(11): 1357–1365. doi:10.1002/nbm.3408.

Dynamic correlations between hemodynamic, metabolic, and neuronal responses to acute whole-brain ischemia

Jennifer M. Taylor, BS[1,2], **Xiao-Hong Zhu, PhD**[1], **Yi Zhang, MD**[1], and **Wei Chen, PhD**[1,2,*]

[1]Center for Magnetic Resonance Research, Department of Radiology, University of Minnesota, Twin Cities, MN

[2]Department of Biomedical Engineering, University of Minnesota, Twin Cities, MN

Abstract

Cerebral ischemia sets off a cascade of neuronal and metabolic responses to preserve brain viability. Understanding the temporal evolution of these changes during and after ischemia, and their correlation to hemodynamic changes, is essential. In this study, a 12-minute whole-brain ischemia based on the 4-blood-vessel-occlusion model was employed in rats. Using a high-temporal resolution simultaneous ^{1}H-^{31}P MRS acquisition sequence at 9.4T, we investigated dynamic occlusion and reperfusion responses in cerebral Lac, PCr, ATP, pH, and BOLD, in complement to changes in neuronal field potential activity. We reveal tightly coupled dynamics between hemodynamic, metabolic and neuronal responses to ischemia. Neuronal activity, BOLD, PCr, Lac, and pH changed immediately following occlusion, indicating reduced energy substrates and consumption, and increased glycolysis to maintain cellular ATP levels, which started to decrease 2.2 minutes after occlusion onset. ATP stores were then gradually consumed to maintain a minimum housekeeping neuronal activity level. By correlating dynamic changes of brain activity, BOLD, and energy metabolism, new insights into the brain's survival ability and mechanisms during an acute ischemic attack from the perspectives of cerebral metabolism, neuroenergetics and neuronal activity were gained.

Graphical abstract

Investigation of rat brain hemodynamic, metabolic, and neuronal activity with high temporal resolution provides new insight into brain dynamics. Here, we study these dynamic changes to ischemia and reperfusion using a 12- minute whole-brain ischemia model. We find that all dynamic changes are highly coupled but with distinct temporal behaviors, particularly for the cellular ATP reserve, which exhibits a significantly delayed response to ischemia.

*Corresponding Author: Wei Chen, PhD, Center for Magnetic Resonance Research, Department of Radiology, University of Minnesota, 2021 6th Street SE, Minneapolis, MN 55455, USA. Fax: 612-626-2004, Phone: 612-626-2001, wei@cmrr.umn.edu.

Conflict of Interest Statement: The authors have no conflict of interest to disclose.

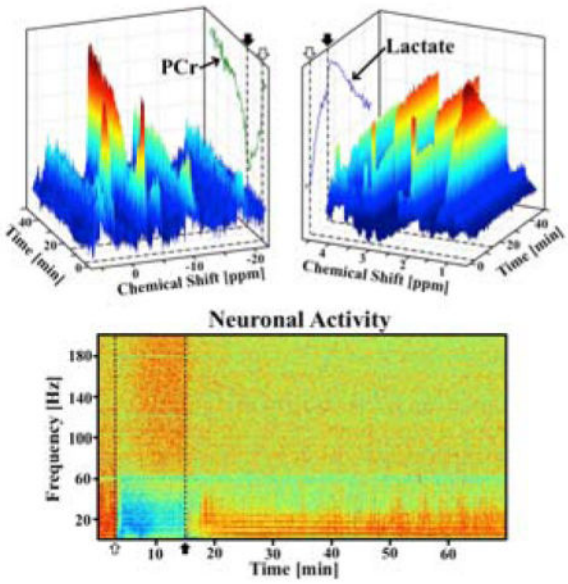

Keywords

Brain metabolism; Brain hemodynamics; Electrophysiology; MR Spectroscopy; Brain ischemia; Simultaneous acquisition

INTRODUCTION

Dynamic magnetic resonance spectroscopy (MRS) provides a wealth of *in vivo* information about brain metabolic pathways, rates, and mechanisms that can be explored utilizing specific nuclear MRS. For example, anaerobic metabolism can be monitored via cerebral lactate (Lac) concentration information with proton (^{1}H) spectroscopy (1–3). Phosphorous (^{31}P) spectroscopy reveals high-energy phosphorous metabolites including PCr and ATP, and possibly the oxidative phosphorylation rate of ADP for producing ATP in mitochondria (3–6).

To better understand the dynamic relationship between metabolic and hemodynamic changes in the rat brain in response to a pathophysiological change, we have developed a high temporal resolution multi-channel MRS pulse sequence capable of acquiring dynamic ^{1}H and ^{31}P spectra simultaneously. From these information-rich signals, we measured the dynamic responses of Lac, PCr, ATP, pH, and blood-oxygenation-level-dependence (BOLD) to an acute 12-minute whole-brain ischemia using the 4-blood-vessel-occlusion model (7,8) with a 32-second temporal resolution. Upon induction of occlusion, the cerebral Lac concentration increases as a byproduct of glycolysis, recovering slowly to baseline following reperfusion, while PCr decreases dramatically upon occlusion and recovers relatively quickly. While these results match the findings of similar ischemia models (1,9–17), increased temporal and spectral resolution at high field allows us to observe a delayed ATP response *in vivo* after the onset of occlusion, and to assess the hemodynamic and metabolic changes of individual animals within a single measurement.

Correlations between neuronal activity, specifically local field potentials, and BOLD responses to a paradigm stimulus have previously been explored using simultaneous electrophysiology and functional MRI methods (18,19). Metabolic activity should play a key role in modulating this link under ischemic condition, but is either explored using *ex vivo* extraction methods or low-temporal resolution *in vivo* MRS. To connect metabolic, hemodynamic, and neuronal activity changes with high temporal resolution, neuronal activity in the rat cortex under the same occlusion and reperfusion protocol was recorded outside of the MRI scanner, and correlated with the MRS measures, including BOLD. This information was used to investigate the cross correlations of both fast and slow dynamic changes of brain metabolism, BOLD, and neuronal activity during and after 12 minutes of whole-brain ischemia with high temporal resolution.

MATERIALS AND METHODS

Animal Surgical Preparation

Whole-brain ischemia was induced in male Sprague-Dawley rats (n = 10, weight: 260 – 400 g). The 4-blood-vessel-occlusion (4BVO) preparation (7,8) was performed in two surgeries 24 to 48 hours apart. In brief, both vertebral arteries were cauterized under sterile surgical conditions. Animals were recovered for 1 – 2 days in a warm cage with soft food available. Hydronic (balloon) occluders (Harvard Apparatus, Holliston, MA) were installed around the common carotid arteries following intubation and femoral artery and vein catheterization. The rats were placed in a supine position on a custom-made MR compatible cradle, and immobilized with ear and bite bars. Occluders were inflated for 12 minutes to induce a reversible occlusion.

During surgery, anesthesia was induced with 5% isoflurane and then maintained at 2%. Animals were kept between 1.6 and 2.0% isoflurane for the entire measurement session. Body temperature was monitored with a rectal probe and maintained at 37°C with a heated water pad. Using a BIOPAC data acquisition system (Goleta, CA), blood pressure was monitored through the femoral artery catheter, and inhaled and exhaled O_2, CO_2, N_2O, and isoflurane levels were sampled and monitored from the intubation line during the entire experiment. Inhaled O_2 and N_2O were kept at a 40:60 ratio. Blood pressure was considered stable if it was constant for 10 minutes, and was 86 ± 26 mmHg prior to occlusion on average. Arterial blood samples were analyzed to monitor pO_2 (158.6 ± 45 mmHg), pCO_2 (35.4 ± 9.5 mmHg), and pH (7.44 ± 0.07). At the end of the study, a heart attack was induced with a high dose bolus of potassium chloride (KCl) through a venous line.

Animals were split into a MRI/MRS group (4 first and 4 second occlusion datasets were collected across 6 animals) and an electrophysiology group (4 first occlusion datasets were collected across 4 animals). In addition to the occluder placement, two small (< 4 mm) bilateral craniotomies were performed on the electrophysiology group to expose the primary somatosensory rat forelimb cortex regions (S1FL) for bilateral placement of two linear array probes. Physiological measurements after surgery were not observed to be different from animals without craniotomies. All animal experiments were conducted according to the National Research Council's Guide for the Care and Use of Laboratory Animals, and under

protocols approved by the Institutional Animal Care and Use Committee of the University of Minnesota.

Occlusion and Reperfusion Protocol

To induce global brain ischemia, the bilateral occluders were inflated for 12 minutes. Changes in systemic blood pressure were used to verify the occlusion based on expectations from literature (7,20). Data acquisition consisted of a 3-minute control period, a 12-minute occlusion, and a 30+ minute reperfusion and recovery period. The occlusion and recording were repeated 30–60 minutes later if the animal's recovery blood pressure level was maintained for at least 10 minutes and was similar to baseline values (average drop 13 ± 32 mmHg), and if brain lactate returned to the pre-ischemic baseline level. After the completion of the occlusion study, the response to an induced heart attack (i.e., no blood circulation) and an *ex vivo* control (dead brain) were acquired.

MRI/MRS Measurements

In vivo MR imaging and spectroscopy was acquired on a 9.4T/31cm horizontal bore magnet (Magnex Scientific) interfaced with a VnmrJ console (Agilent Technologies, Santa Clara, CA). A dual-tuned radio-frequency (RF) surface coil was used, comprised of a butterfly ^{1}H coil and single loop ^{31}P coil (12 mm × 20 mm oval).

Similar to techniques previously shown (12,17,21–23), we combined two MRS acquisition sequences within a single TR, allowing simultaneous acquisitions of ^{1}H and ^{31}P spectral signals. Spectral SNR and temporal signal fluctuations between repeated measurements were verified for the multi-channel sequence acquisitions as equivalent to single channel acquisitions. For this study, the localized ^{1}H spectroscopy sequence PRESS (24) (TR = 4 s, TE = 15 ms, voxel size: 5×4×5 mm^{3}) was combined with a global ^{31}P single pulse (SPULS) acquisition. A nominal 90° RF pulse was employed to optimize the ^{31}P signal detection from the rat brain. VAPOR water suppression (25) was employed prior to the ^{1}H PRESS sequence, and localized shimming was performed with FASTMAP (26). Spectra were averaged over 8 acquisition blocks (i.e., N=8) to increase SNR, giving a final temporal resolution of 32 seconds. Data was excluded if high lipid contamination remained in the ^{1}H spectrum.

Electrophysiology Recording

Electrophysiology data was acquired continuously at 2 kHz using a Cerebus Acquisition System (Blackrock Microsystems, Salt Lake City, UT) on 64 channels across two 32-channel linear array probes (NeuroNexus, Ann Arbor, MI) to monitor field potential activity in S1FL cortex. Signal quality was visually verified during the experiment, and the suppression of neuronal bursting activity was used to verify a successful occlusion.

Spectral Analysis

Manual spectral phasing was performed in VnmrJ (Agilent Technologies, Santa Clara, CA) on a 5-minute averaged baseline spectrum for each rat (Fig. 1A,B). Individual spectrum quality as well as temporal stability can be observed in the dynamic spectral trends in response to occlusion and reperfusion in Fig. 1C,D. Spectral quantification was performed

using custom MATLAB (MathWorks, Natick, MA) code. Based on the finding of stable Cr concentration during and following occlusion by Nagatoma *et al* (9), a baseline total creatine concentration ($[Cr]_{total}$, including Cr and PCr) of 8.5 mM (27) was used for the normalization and quantification of [Lac], and the BOLD-effect was calculated from the percentage change in the linewidth of the Cr resonance at 3 ppm (28,29). Each ^{1}H spectrum was then corrected for this BOLD-effect prior to [Lac] quantification. To minimize lipid and macromolecule contributions in the [Lac] quantification, baseline ^{1}H spectra were averaged for each rat and subtracted from dynamic spectra measured during occlusion and post-ischemia reperfusion. The subtracted Lac peak was integrated to give changes in [Lac] (ΔLac, mM). Baseline [PCr] detected by ^{31}P MRS was normalized to 3.9 mM (27), and Lorentzian fitting and integration was performed on the PCr peak (−2.5 ppm, Fig. 1A) for the quantification of dynamic changes (ΔPCr, mM). While the global ^{31}P signal could include small contributions from the surrounding muscle, the entire signal was assumed to be dominant by brain tissue to simplify analysis.

Additionally, ^{31}P spectra were averaged at each time point across all 8 occlusions among the 6 rats in the MRI/MRS experiment group to increase SNR for reliable fitting of the γ-ATP resonance peak (−5 ppm, Fig. 1A) and for the identification of changes in the chemical shift of inorganic phosphate (Pi). From these average spectra, group ΔPCr and ΔATP were quantified by integrating their respective spectral peaks, then compared to the baseline PCr integral and [PCr] = 3.9 mM. The intracellular pH values were calculated (11) using the equation

$$pH = 6.75 + log\left(\frac{\Delta\delta - 3.29}{5.7 - \Delta\delta}\right), \quad \text{(Eqn. 1)}$$

where Δδ is the chemical shift difference in parts per million (ppm) units between the PCr and Pi peaks. Justification for averaging across occlusions will be addressed in the **RESULTS & DISCUSSION** section.

A coupled piecewise function consisting of a flat baseline and exponential occlusion and recovery phases was fitted to the temporal trend of each MRS metabolite of interest, following the equation

$$y(t) = \begin{cases} c_{Baseline}, & 0 < t \le t_1 \\ (a * exp(-k * t) + c)_{Occlusion}, & t_1 < t \le t_2 \\ (a * exp(-k * t) + c)_{Reperfusion}, & t > t_2 \end{cases} \quad \text{(Eqn. 2)}$$

where t is time, k is a rate constant, a and c are offset constants, t_1 is the occlusion-induced change start time, and t_2 is the reperfusion-induced change start time. A reasonable delay following occlusion induction and release was allowed for the fitting of t_1 and t_2. A second recovery phase was added for pH to improve regression fit accuracy (Root-mean-squared-error, RMSE, of 1 Phase: 0.091 versus 2 Phases: 0.069). An example of the PCr and Lac fit is shown in Fig. 2A. Fitted Lac and PCr results from the same occlusion measurement were plotted against each other to examine temporal trends.

Electrophysiology Analysis

Continuous electrophysiology data was notch-filtered for 60 Hz noise prior to analysis. Time-frequency spectrograms (0 – 200 Hz) for each electrode channel were used to calculate signal power. Frequency normalization was performed to remove the 1/f power dependence (30) and improve visualization of time-domain dynamics. Multi-unit and spike activity were not analyzed here, as the deep isoflurane anesthesia level resulted in a very low spike detection rate. Temporal data was averaged across four frequency bands: 0 – 10 Hz (Low Frequency, LF), 10 – 30 Hz (Medium Frequency, MF), 30 – 58 Hz (Low Gamma, LG), and 62 – 200 Hz (High-Gamma, HG). For compatibility with the large brain volume MRS data, and utilizing the widespread, less specific neuronal connectivity under deep isoflurane anesthesia (31), the power of the field potentials was averaged across all channels within each rat. Traces were temporally smoothed with a 1-minute sliding window.

Statistical Analysis

Analysis values are given as *mean* ± *standard deviation* (SD). A linear mixed model was used when comparing the same metabolite to account for occlusion order, while correlations were used for comparing different metabolites time courses. Statistical significance was achieved for $p < 0.05$, unless otherwise stated. Correlation coefficients were considered highly significant for $|r| > 0.8$ and a $p < 0.001$.

RESULTS & DISCUSSION

MRS Data Quality

Simultaneously acquired *in vivo* ^{1}H-^{31}P dual-nuclei MRS spectra have the same SNR as acquisition with traditional single-nucleus acquisition methods. The SNR and spectral resolution of our ultra-high field ^{31}P and ^{1}H spectra can be seen in representative baseline spectra (Fig. 1A–B, respectively). The temporal and spectra SNR of dynamically acquired data during an occlusion and reperfusion can be seen in Fig. 1C and 1D for ^{31}P and ^{1}H, respectively.

Metabolic and BOLD Responses to Ischemia

The 4BVO occlusion model produces a whole-brain ischemia, resulting in a large oxygen and energy deficiency in the rat brain. The occlusion onset immediately induces reductions in PCr and BOLD signals, and an increase in Lac (Fig. 1C–D, Fig. 2A–B). Reperfusion reverses these trends, although with a slower Lac recovery rate. Similar trends are observed upon heart attack induction and complete suppression of blood circulation, but with a larger PCr drop (Fig. 2A) indicating that some energy reserves and residual blood flow remained during occlusion. In contrast, a relatively lower maximal ΔLac was induced by the heart attack and brain death as compared to the occlusion (Fig. 2A), pointing to the depletion of glycogen reserves during the 12-minute occlusion.

Quantification of metabolic exponential regression rates (k from Eqn. 2) highlights differences in the PCr and Lac responses, as well as differences between occlusion, reperfusion, and heart attack. The rate of PCr change for the occlusion ($k = 0.27 \pm 0.2$) was not statistically different from that of reperfusion ($k = 0.38 \pm 0.21$, $p > 0.05$). Lac reduced

slower following reperfusion ($k = 0.04 \pm 0.05$, approaching linear) than it increased during occlusion ($k = 0.19 \pm 0.07$), although the difference did not reach statistical significance. The difference of Lac responses between occlusion and reperfusion may result from the interplay between Lac transport across the blood brain barrier, the washout removal of excessive brain Lac, and possible cerebral Lac metabolism (2). The significant increase in Lac production rate following heart attack induction ($k = 0.57 \pm 0.38$, $p < 0.05$), compared with occlusion and recovery, highlights the presence of residual blood flow from peripheral vessels during occlusion in comparison with the complete absence of blood supply after the heart attack, as well as the response dependence on occlusion model.

The simultaneous nature of this ^{1}H-^{31}P MRS acquisition allows the analysis of PCr and Lac in the same rat within a single occlusion, previously assumed to have consistent trends across multiple rats. Analysis of simultaneous MRS data reveals that the individual PCr responses to occlusion and recovery were much more similar than Lac responses which showed more variation between inter-subjects. Figure 3A shows the time courses of the Δ[Lac]/ [PCr] ratio for each rats. Within these ratio traces, two groups with different magnitudes of ratio changes were observed. Performing a post-hoc linear mixed model test on the area-under-the-curve of the ratio traces, the observed groups were determined them to be statistically different ($p = 0.001$). Differences between these two groups are highlighted by plotting Lac versus PCr correlation loops, viewed clockwise (Fig. 3B–C), showing clearly that the trends between the two groups were dominated by the larger Δ[Lac] variation among different rats. Notice that the shape of the correlation curves are more consistent for the first trend than the second, as well as smaller end changes in Lac and PCr.

Considering the brain as a closed system during a complete whole-brain occlusion with no blood flow and thus no influx or efflux of nutrients including oxygen, glucose, and lactate, a simplified glycolysis metabolic model was employed to estimate the maximal Lac change resulting from the occlusion. Using the literature concentration values of 10 mM blood glucose, 2 mM brain tissue glucose, and 4 mM glycogen (32,33), and approximating a 5% brain blood volume, it can be estimated that a maximum of 12.4 mM of Lac can be generated from the consumption of all available glucose and glycogen substrate pools in the rat brain. While in reality residual blood flow was present, the maximal Lac of 13.2 mM for Trend 1 is closer to this prediction than that of 7.8 mM for Trend 2. It is therefore hypothesized that occlusion in Trend 2 had reduced metabolic energy reserve pools of glucose and glycogen as compared to Trend 1. Blood glucose levels have previously been connected with increased ischemia impact (15,34,35). It was observed that some rats remained lethargic following the initial surgery, and may have had low energy reserves, although weight loss did not correlate with final lactate results. Alternatively, Trend 2 occlusions may have had increased peripheral vessel blood flow, however a very small, non-significant correlation coefficient of −0.23 ($p = 0.58$) between maximal changes in Lac versus BOLD does not support this notion. Further investigation is needed to distinguish the true metabolic basis for Trend 2.

Ischemia Induced Neuronal Field Potential Responses

The temporal dynamics of the neuronal field potential response to occlusion reveal a rapid reduction in signal power across 0 – 200 Hz for the first 2 minutes of occlusion, with a small amount of recovery during the second half of occlusion in some electrode recording channels. Signal power recovers further following reperfusion but does not reach baseline levels. The deep 1.6–2.0% isoflurane anesthesia used here results in an unconscious state in the rat brain with typical burst-suppression EEG patterns (31) (Fig. 4A–a). Occlusion and reperfusion induced changes in burst signal amplitudes and duration in the temporal domain can be observed in Fig. 4A, and match the trends seen in the average field potential power spectrum curves (Fig. 4B). Field potential power following heart attack induction (dead brain representing the EEG background noise level, Fig. 4A–d) can be seen to be substantially lower than occlusion (Fig. 4A–b and Fig. 4B), again indicating some residual metabolic energy, blood flow, and neuronal activity during occlusion despite the lack of neuronal bursting activity. The field potential power amplitudes follow the order of baseline (highest), post-ischemia recovery, occlusion, and dead brain across a wide range of frequencies (Fig. 4B).

Group Comparison of Metabolic, BOLD, and Neuronal Responses

Beyond PCr, other energy molecules observable with ^{31}P MRS provide additional insights into cerebral energetics, but the SNR within the ^{31}P spectra of a single rat is insufficient for reliable quantification of low concentration metabolites such as Pi. Averaging the ^{31}P spectra at each measurement time point across all rats produced sufficient SNR for group quantification, comparison, and exponential regression fitting of cerebral PCr, ATP, and intracellular pH dynamics (Fig. 5A–D). Group averaged PCr displays the same trend as individual rats, immediately dropping upon occlusion onset until reperfusion, showing a similar recovery rate to the baseline level during reperfusion.

While different vasculature responses from repeated occlusions have been observed in the literature (20), no dependence on occlusion order was observed in the metabolic time courses in the present study, presumably owing to a small sample size and mild impairment with a relatively short occlusion. Only a slight difference in the ΔPCr response to the first occlusion versus second occlusion was observed, where the maximum reduction by the end of the 12-minute occlusion period was slightly larger for the second than the first occlusion (Fig. 3B). A linear mixed model with Bonferroni correction did not find a statistical significance between PCr responses of Occlusion 1 versus Occasion 2 ($p = 0.002$, Bonferroni significance at $p = 5.8e^{-4}$). Differences were only seen in the recovery phase (paired t-test, $p < 0.05$ for the initial recovery period of 20–35 minutes, $p > 0.05$ otherwise). These differences are consistent with a second occlusion that is metabolically slightly more severe than the first, as well as indicating the possibility of depleted glycogen reserves after the first occlusion. Averaging both occlusion responses together will slightly pull the data towards a middle range of occlusion severity, which given inter-animal variability and unknown residual perfusion, is still generally comparable. Results of other metabolite dynamics would therefore be slightly less severe than average for the first occlusion, and slightly more severe for the second occlusion.

Interestingly, ATP dynamics had a 2.2-minute delayed reduction response to occlusion, and the reperfusion steady state of [ATP] was significantly lower than baseline ($p = 8.3e^{-4}$), at 80% (Fig. 5B). To our knowledge, this short delay in ATP response has not been previously observed *in vivo* in the literature with limited sensitivity and temporal resolution of *in vivo* ^{31}P MRS. In a decapitation model by Lowry *et al* (14), a plot of [ATP] and other metabolites shows ATP remaining near baseline for approximately 2 minutes in anesthetized mice, however this delay could be seen as noise in the data, and the authors did not discuss the biological significance. Indirect support of this delay can be also found in the brain slice model used by Fleidervish *et al* (36), where an increase in ATP-sensitive potassium channel activation was observed 3 minutes into hypoxia. Additionally, Raffin *et al* observed a latency of extracellular anoxic depolarization of 122 s, on average, which they linked to brain energy deprivation (37). Bainbridge *et al* (10) found a change in ATP (referred to as NTP) decline associated with PCr reaching 1/3 of the baseline values, however the time of occurrence appears to be much later than our results and the authors did not discuss or quantify this time point. This difference could be attributed to different animal and ischemic models.

As anticipated, changes in pH (Fig. 5C) were found to mirror that of Lac (Fig. 5D, $r = -0.86$, $p = 3e^{-25}$), responding immediately to occlusion, but with a delay of 1.8 and 1.5 minutes to reperfusion, respectively. Lac and pH trends diverged 10 minutes post-reperfusion, with pH following a distinct additional exponential recovery trend. This divergence time point matches when the recoveries of PCr and ATP concentrations recovered to a steady-state level (Fig. 5A–B), and may be indicative of a complex but interesting relationship between the ATP energy reserves, cell acidity, and lactate concentration. In contrast to the metabolic responses, the average BOLD response (Fig. 5E) reached a low steady state within 1 minute of occlusion, staying there until reperfusion, with a short (~2 minutes) recovery period back to baseline, and the BOLD change exhibited no strong correlation with other metabolites, presumably owing to the distinct dynamics between the fast hemodynamic change which dominates the BOLD signal and relatively slow energy metabolites responses. While the overall trend of these metabolite changes match that previously found separately in literature (11,12,17), the high temporal resolution and simultaneous ^{1}H-^{31}P MRS measurements reported herein allow *in vivo* assessment of the short delays and dynamic correlations among metabolites and BOLD changes.

Multi-channel and multi-rat averaged responses of field potential spectral power were split into four frequency bands (see **MATERIALS AND METHODS**) to highlight group neuronal responses (Fig. 5F). The field potential power in the LF and MF bands quickly dropped to 40% of baseline level upon occlusion, and to approximately 60% for the LG band, tightly linking neuronal activity to the reduced oxygen supply (37). Interestingly, despite this link and the band activity visually following the average BOLD dynamics (Fig 5E), the LG band was found to be more closely correlate with BOLD ($r = -0.69$, $p = 4.3e^{-13}$). These activities reached a new low steady state within 2 minutes, around the same time as ATP began to be depleted (Fig. 5B). The similar dynamics and time scales between the neuronal activity and brain ATP changes clearly suggest an essential role of cellular ATP availability in supporting neuronal activity and function under the rest as well as

neuronal impairment and dysfunction under the ischemic attack. This significance of the 2-minute delay is highlighted by the observation of Pulsinelli *et al* (7), where awake animals became unresponsive with isoelectric EEG at 2–3 minutes following an occlusion using the same 4BVO model. Interestingly, the changes in HG are much smaller, showing opposite changes to the systemic blood pressure response (Fig. 2C), with under- and over- shooting after paradigm (occlusion and reperfusion) changes. Higher frequency neuronal activity originates from local neuron recruitment (30), possibly reflecting the initial disruption of hypoxia on small local networks. None of the frequency bands analyzed returned to baseline power levels. Despite this, the animals in the study by Pulsinelli *et al* (38) did not show abnormal behavior following recovery, and neuronal ischemic damage was delayed on the order of hours. Schmidt-Kastner *et al* (13) reported EEG traces returned to normal 72 hours following occlusion, both far beyond the time frame monitored in our present study. These findings could explain the majority of similar changes between the first and second occlusions as observed in the present study.

Analysis of group responses to occlusion and reperfusion revealed strong correlations ($|r| > 0.8$, all with $p < 0.001$) between neuronal and metabolic changes. Both pH and PCr had correlations of greater than 0.8 to LF ($r = 0.87$ and 0.86) and MF ($r = 0.83$ and 0.81) bands of the neuronal power. Correspondingly, there was a strong correlation between pH and PCr ($r = 0.82$, $p = 7.6e^{-22}$). As mentioned previously, lactate and pH were also inversely correlated ($r = -0.85$), as expected from the acidic nature of lactate. BOLD was not strongly correlated with any other measure, presumably due to a fast reduction in response to occlusion.

Pulling all of these dynamic responses together, our high temporal resolution simultaneous ^{1}H-^{31}P measurement allows a cause-and-effect flow to be extrapolated. Upon the occlusion onset, BOLD decreases dramatically due to the rapid and substantial reduction of blood supply and perfusion, resulting in an increase in highly deoxygenated hemoglobin. This BOLD measure is mainly determined by the hemodynamic or perfusion changes during and after the 12-minute occlusion. Field potential power activity closely follows the changes in blood flow and BOLD, showing immediate suppression after the onset of occlusion. This suggests a tightly coupled neuro-vascular relationship, as seen previously (37). The rapid metabolic switch to glycolysis triggered by the lack of oxygen supply during occlusion, where PCr reserves are consumed at a constant decay rate to maintain ATP following occlusion onset, results in Lac byproducts and a change in pH within 30 seconds, or one MRS data point. ATP stores are tapped 2 minutes after occlusion induction, when low-frequency field potential powers and BOLD reach low steady states, indicating the need for the brain to maintain a minimum neuronal activity level, and relating to the maintenance of the basic housekeeping brain energy proposed by Attwell *et al* (39), Du *et al* (6), and Howarth *et al* (40). Energy metabolites continue to decrease throughout the 12-minute occlusion, reaching a pseudo steady state as the occlusion release time-point is approached. Particularly in comparison with dead brain signal measures, the very low neuronal activity and metabolic concentration levels needed to maintain this housekeeping energy reveals the brain’s robustness to harsh conditions.

The return of blood flow is reflected in an immediate recovery of BOLD, returning to baseline within 2 minutes. PCr, ATP, and field potential power begin to recover without a delay, but at a much slower rate than BOLD. In contrast, the recovery of Lac and pH is delayed 1.5 – 2 minutes, likely as a result of continued glycolysis in order to return ATP and PCr to a normal concentration range. The slow recovery of Lac to its baseline level points to a dominant but slow Lac transport efflux and blood flow washout as opposed to an active metabolic breakdown. The PCr recovery to a steady state was not significantly different from pre-occlusion baseline ($p = 0.79$), while ATP did not recover to baseline ($p = 8.3e^{-4}$), staying at 80% of baseline, with their recovery mainly occurring within 10 minutes following reperfusion. The small differences in the degree of PCr recovery to baseline for first versus second occlusion would not raise this group ATP recovery baseline to 100% if the occlusions were quantified for each occlusion group separately. This persistent ATP depletion during the reperfusion period, though small, may contribute to the increased severity of the second occlusion. LF, LG, and MF field potential bands reached a steady state at 70% of baseline shortly after, followed by pH and Lac returning slowly to baseline. Interestingly, most physiological measures gradually recovered to the baseline levels during the reperfusion period, however, both ATP and neuronal activities remained below the baseline levels. This finding again indicates a tight coupling relationship between the brain ATP availability and neuronal activity impairment.

The results and temporal correlations among multiple neurophysiological measures collectively suggest that the cellular ATP availability and production through oxidative phosphorylation in mitochondria and its dynamics have a major influence on the outcome and temporal behavior of other physiological changes, in particular, neuronal field potentials and tissue pH. From a neuroenergetic perspective, oxygen metabolism is most essential for ATP generation, since the metabolism of a single glucose molecule can generate more than 30 ATP molecules via oxygen metabolism, as compared to only 2 ATP via the glycolysis. The total oxygen stored in the brain tissue is very limited, and can only sustain cerebral oxygen metabolism for less than 30 seconds if the arterial oxygen supply is completely stopped due to the occlusion. Therefore, PCr plays an immediate role in supporting the ATP energy conversion, and meanwhile, the glycolysis metabolism of the tissue glucose and glycogen reserves was enhanced to produce ATP energy during the ischemic challenge though with low efficiency. Therefore, we hypothesize that the delay time of brain ATP level reduction after the onset of ischemic insult should provide a sensitive measure of the ischemic severity, and reflects the outcome of highly coupled dynamics among hemodynamic, metabolic, and neuronal activity responses.

CONCLUSION

While displaying temporally different trends, the dynamic changes of hemodynamic, metabolic, and neuronal activity during whole-brain ischemia and reperfusion are tightly related in general, and are crucial for cell viability and survival of the insult. High temporal resolution simultaneous multi-channel MRS acquisition is a powerful tool to investigate these dynamic responses. In this study, we have shown that this advanced MRS technique is capable of quantitatively revealing dynamics and correlations between Lac and PCr changes within a single animal brain. Group comparison of Lac, PCr, ATP, pH, and BOLD with

neuronal field potential power bands highlights the importance of a tight neuronal-vascular coupling to conserve metabolic energy stores during the extremely hypoxic state. We observe, for the first time *in vivo*, a 2.2-minute conservation of cerebral ATP levels, a potentially important time-point related to the minimal neuronal activity levels required to allow functional recovery upon reperfusion. The overall results provide new insights into a comprehensive and dynamic relationship between neuronal activity, brain hemodynamic, and metabolic changes in response to an acute ischemia and during post-ischemic reperfusion.

Acknowledgments

This work is supported in part by NIH grants NS057560, NS041262, NS070839, P41 RR008079 & EB015894, P30 NS057091 & NS5076408, and the Keck Foundation. The authors thank Drs. Ivan Tkac and Steve Suddarth for technical support.

Abbreviations

^{1}H	proton nucleus
^{31}P	phosphorous nucleus
4BVO	4-blood-vessel-occlusion
HG	High gamma band (62–200 Hz)
LF	Low frequency band (0–10 Hz)
LG	Low gamma band (30–58 Hz)
MF	Medium frequency band (10–30 Hz)

References

1. Malisza KL, Kozlowski P, Peeling J. A review of *in vivo* ^{1}H magnetic resonance spectroscopy of cerebral ischemia in rats. Biochem Cell Biol. 1998; 76(2–3):487–496. [PubMed: 9923718]
2. Howe FA, Maxwell RJ, Saunders DE, Brown MM, Griffiths JR. Proton spectroscopy *in vivo*. Magn Reson Q. 1993; 9(1):31–59. [PubMed: 8512831]
3. Kemp GJ, Radda GK. Quantitative interpretation of bioenergetic data from ^{31}P and ^{1}H magnetic resonance spectroscopic studies of skeletal muscle: an analytical review. Magn Reson Q. 1994; 10(1):43–63. [PubMed: 8161485]
4. Ackerman JJ, Grove TH, Wong GG, Gadian DG, Radda GK. Mapping of metabolites in whole animals by ^{31}P NMR using surface coils. Nature. 1980; 283(5743):167–170. [PubMed: 7350541]
5. Chen W, Zhu X-H, Adriany G, Uğurbil K. Increase of creatine kinase activity in the visual cortex of human brain during visual stimulation: A ^{31}P NMR magnetization transfer study. Magn Reson Med. 1997; 38(4):551–557. [PubMed: 9324321]
6. Du F, Zhu XH, Zhang Y, Friedman M, Zhang N, Ugurbil K, Chen W. Tightly coupled brain activity and cerebral ATP metabolic rate. Proc Natl Acad Sci U S A. 2008; 105(17):6409–6414. [PubMed: 18443293]
7. Pulsinelli WA, Brierley JB. A new model of bilateral hemispheric ischemia in the unanesthetized rat. Stroke. 1979; 10(3):267–272. [PubMed: 37614]
8. Sugio K, Horigome N, Sakaguchi T, Goto M. A model of bilateral hemispheric ischemia--modified four-vessel occlusion in rats. Stroke. 1988; 19(7):922–922. [PubMed: 3388463]

9. Nagatomo Y, Wick M, Prielmeier F, Frahm J. Dynamic monitoring of cerebral metabolites during and after transient global ischemia in rats by quantitative proton NMR spectroscopy *in vivo*. NMR Biomed. 1995; 8(6):265–270. [PubMed: 8732182]
10. Bainbridge A, Tachtsidis I, Faulkner SD, Price D, Zhu T, Baer E, Broad KD, Thomas DL, Cady EB, Robertson NJ, Golay X. Brain mitochondrial oxidative metabolism during and after cerebral hypoxia-ischemia studied by simultaneous phosphorus magnetic-resonance and broadband near-infrared spectroscopy. Neuroimage. 2013
11. Bolas NM, Rajagopalan B, Mitsumori F, Radda GK. Metabolic changes during experimental cerebral ischemia in hyperglycemic rats, observed by ^{31}P and ^{1}H magnetic resonance spectroscopy. Stroke. 1988; 19(5):608–614. [PubMed: 3363594]
12. Rudin M, Sauter A. Dihydropyridine calcium antagonists reduce the consumption of high-energy phosphates in the rat brain. A study using combined ^{31}P/^{1}H magnetic resonance spectroscopy and ^{31}P saturation transfer. J Pharmacol Exp Ther. 1989; 251(2):700–706. [PubMed: 2810119]
13. Schmidt-Kastner R, Paschen W, Ophoff BG, Hossmann KA. A modified four-vessel occlusion model for inducing incomplete forebrain ischemia in rats. Stroke. 1989; 20(7):938–946. [PubMed: 2749852]
14. Lowry OH, Passonneau JV, Hasselberger FX, Schulz DW. Effect of Ischemia on Known Substrates and Cofactors of the Glycolytic Pathway in Brain. J Biol Chem. 1964; 239:18–30. [PubMed: 14114842]
15. Ljunggren B, Norberg K, Siesjo BK. Influence of tissue acidosis upon restitution of brain energy metabolism following total ischemia. Brain Res. 1974; 77(2):173–186. [PubMed: 4852452]
16. Gyulai L, Schnall M, McLaughlin AC, Leigh JS Jr, Chance B. Simultaneous ^{31}P- and ^{1}H-nuclear magnetic resonance studies of hypoxia and ischemia in the cat brain. J Cereb Blood Flow Metab. 1987; 7(5):543–551. [PubMed: 3654794]
17. Chang LH, Shirane R, Weinstein PR, James TL. Cerebral metabolite dynamics during temporary complete ischemia in rats monitored by time-shared ^{1}H and ^{31}P nmr spectroscopy. Magn Reson Med. 1990; 13(1):6–13. [PubMed: 2319935]
18. Logothetis NK, Pauls J, Augath M, Trinath T, Oeltermann A. Neurophysiological investigation of the basis of the fMRI signal. Nature. 2001; 412(6843):150–157. [PubMed: 11449264]
19. Scholvinck ML, Maier A, Ye FQ, Duyn JH, Leopold DA. Neural basis of global resting-state fMRI activity. Proc Natl Acad Sci U S A. 2010; 107(22):10238–10243. [PubMed: 20439733]
20. Tomida S, Nowak TS Jr, Vass K, Lohr JM, Klatzo I. Experimental model for repetitive ischemic attacks in the gerbil: the cumulative effect of repeated ischemic insults. J Cereb Blood Flow Metab. 1987; 7(6):773–782. [PubMed: 3693433]
21. Eleff SM, Schnall MD, Ligetti L, Osbakken M, Subramanian H, Chance B, Leigh JS. Concurrent measurements of cerebral blood flow, sodium, lactate, and high-energy phosphate metabolism using ^{19}F, ^{23}Na, ^{1}H, and ^{31}P nuclear magnetic resonance spectroscopy. Magn Reson Med. 1988; 7(4):412–424. [PubMed: 3173056]
22. Price TB, Perseghin G, Duleba A, Chen W, Chase J, Rothman DL, Shulman RG, Shulman GI. NMR studies of muscle glycogen synthesis in insulin-resistant offspring of parents with non-insulin-dependent diabetes mellitus immediately after glycogen-depleting exercise. Proc Natl Acad Sci U S A. 1996; 93(11):5329–5334. [PubMed: 8643574]
23. Meyerspeer M, Kemp GJ, Mlynarik V, Krssak M, Szendroedi J, Nowotny P, Roden M, Moser E. Direct noninvasive quantification of lactate and high energy phosphates simultaneously in exercising human skeletal muscle by localized magnetic resonance spectroscopy. Magn Reson Med. 2007; 57(4):654–660. [PubMed: 17390348]
24. Bottomley PA. Spatial Localization in NMR Spectroscopy in Vivo. Ann NY Acad Sci. 1987; 508(1 Physiological):333–348. [PubMed: 3326459]
25. Tkac I, Starcuk Z, Choi IY, Gruetter R. *In vivo* ^{1}H NMR spectroscopy of rat brain at 1 ms echo time. Magn Reson Med. 1999; 41(4):649–656. [PubMed: 10332839]
26. Gruetter R. Automatic, localized *in vivo* adjustment of all first- and second-order shim coils. Magn Reson Med. 1993; 29(6):804–811. [PubMed: 8350724]

27. Pfeuffer J, Tkáč I, Provencher SW, Gruetter R. Toward an *in Vivo* Neurochemical Profile: Quantification of 18 Metabolites in Short-Echo-Time ^{1}H NMR Spectra of the Rat Brain. J Magn Reson. 1999; 141(1):104–120. [PubMed: 10527748]
28. Zhu X-H, Chen W. Observed BOLD effects on cerebral metabolite resonances in human visual cortex during visual stimulation: a functional ^{1}H MRS study at 4 T. Magn Reson Med. 2001; 46(5):841–847. [PubMed: 11675633]
29. Mangia S, Tkac I, Gruetter R, Van De Moortele PF, Giove F, Maraviglia B, Ugurbil K. Sensitivity of single-voxel ^{1}H-MRS in investigating the metabolism of the activated human visual cortex at 7 T. Magn Reson Imaging. 2006; 24(4):343–348. [PubMed: 16677939]
30. Demanuele C, James CJ, Sonuga-Barke EJ. Distinguishing low frequency oscillations within the 1/f spectral behaviour of electromagnetic brain signals. Behav Brain Funct. 2007; 3:62. [PubMed: 18070337]
31. Liu X, Zhu X-H, Zhang Y, Chen W. Neural origin of spontaneous hemodynamic fluctuations in rats under burst-suppression anesthesia condition. Cereb Cortex. 2011; 21(2):374–384. [PubMed: 20530220]
32. Du F, Zhang Y, Iltis I, Marjanska M, Zhu X-H, Henry P-G, Chen W. *In vivo* proton MRS to quantify anesthetic effects of pentobarbital on cerebral metabolism and brain activity in rat. Magn Reson Med. 2009; 62(6):1385–1393. [PubMed: 19780161]
33. Morgenthaler FD, Koski DM, Kraftsik R, Henry P-G, Gruetter R. Biochemical quantification of total brain glycogen concentration in rats under different glycemic states. Neurochem Int. 2006; 48(6–7):616–622. [PubMed: 16522343]
34. Duverger D, MacKenzie ET. The quantification of cerebral infarction following focal ischemia in the rat: influence of strain, arterial pressure, blood glucose concentration, and age. J Cereb Blood Flow Metab. 1988; 8(4):449–461. [PubMed: 2968987]
35. Hoxworth JM, Xu K, Zhou Y, Lust WD, LaManna JC. Cerebral metabolic profile, selective neuron loss, and survival of acute and chronic hyperglycemic rats following cardiac arrest and resuscitation. Brain Res. 1999; 821(2):467–479. [PubMed: 10064834]
36. Fleidervish IA, Gebhardt C, Astman N, Gutnick MJ, Heinemann U. Enhanced spontaneous transmitter release is the earliest consequence of neocortical hypoxia that can explain the disruption of normal circuit function. J Neurosci. 2001; 21(13):4600–4608. [PubMed: 11425888]
37. Raffin CN, Harrison M, Sick TJ, Rosenthal M. EEG suppression and anoxic depolarization: influences on cerebral oxygenation during ischemia. J Cereb Blood Flow Metab. 1991; 11(3):407–415. [PubMed: 1849909]
38. Pulsinelli WA, Brierley JB, Plum F. Temporal profile of neuronal damage in a model of transient forebrain ischemia. Ann Neurol. 1982; 11(5):491–498. [PubMed: 7103425]
39. Attwell D, Laughlin SB. An energy budget for signaling in the grey matter of the brain. J Cereb Blood Flow Metab. 2001; 21(10):1133–1145. [PubMed: 11598490]
40. Howarth C, Gleeson P, Attwell D. Updated energy budgets for neural computation in the neocortex and cerebellum. J Cereb Blood Flow Metab. 2012; 32(7):1222–1232. [PubMed: 22434069]

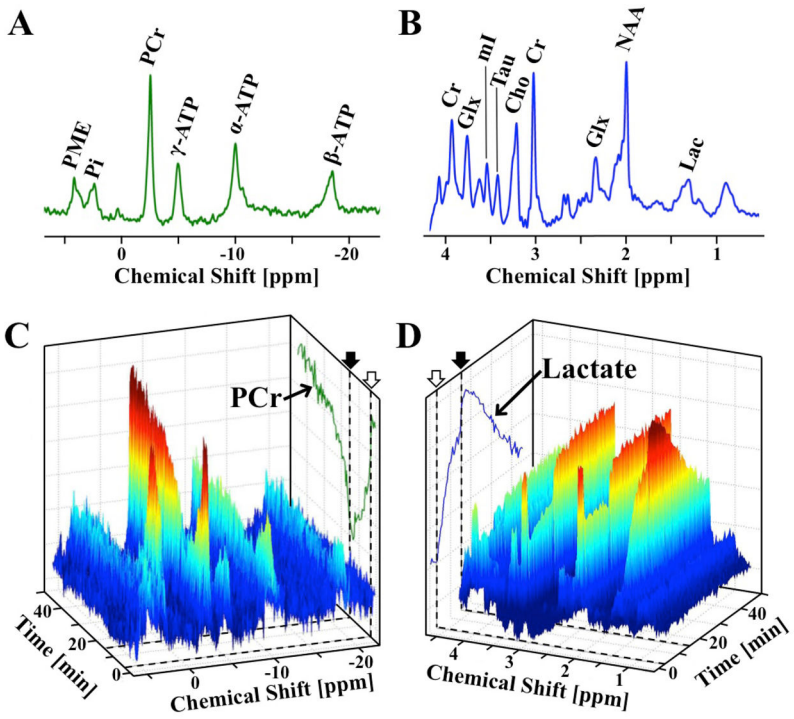

Figure 1.

Representative averaged ultrahigh-field (A) ^{31}P and (B) ^{1}H baseline spectra from a representative rat brain, with major metabolites labeled. Spectral changes of dynamic (C) ^{31}P and (D) ^{1}H spectra during and following ischemia. Occlusion start (open arrow) and release (filled arrow) are indicated by dashed lines on (A, trace) PCr and (B, trace) Lac intensity projections. Temporal resolution is 32 seconds. The BOLD effect on the resonance linewidth and intensity is apparent in the NAA and Cr signals, as well as the lactate projection, particularly at occlusion onset and release.

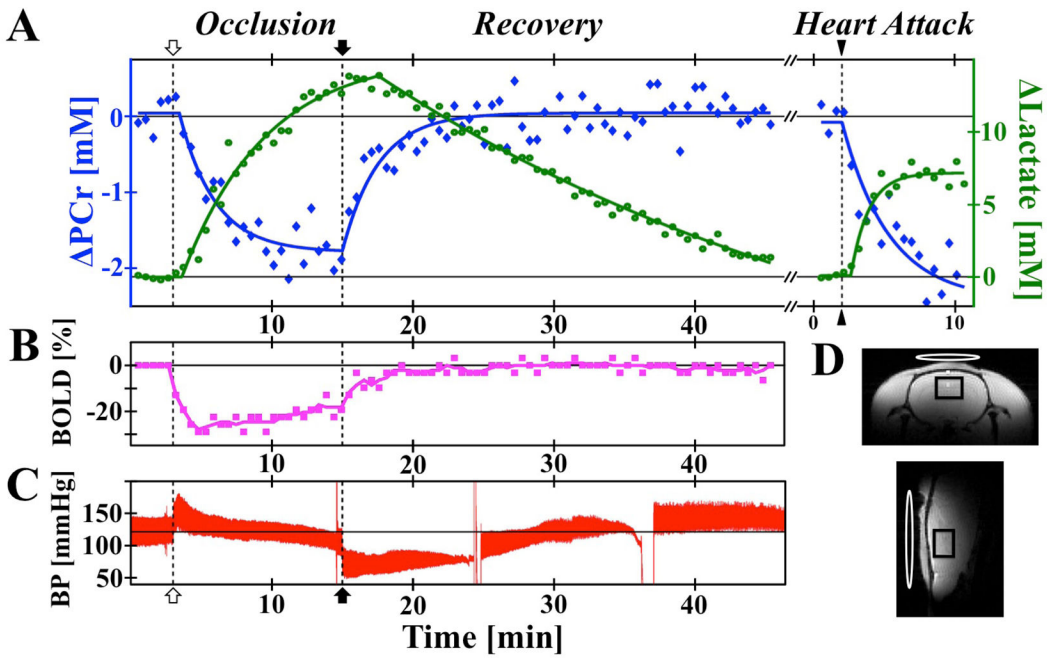

Figure 2.

(A) Representative PCr (blue), Lac (green), (B) BOLD-effect (pink), and (C) blood pressure changes (red) during ischemia, reperfusion, and heart attack, with 32 sec temporal resolution. Solid traces in Lac and PCr indicate exponential regression fits. Occlusion start (open arrow), release (closed arrow), and KCl injection (triangle) indicated with dashed vertical lines. (D) Anatomical imaging in two orientations with black PRESS voxel and white ^{31}P single-loop coil (12 mm × 20 mm oval).

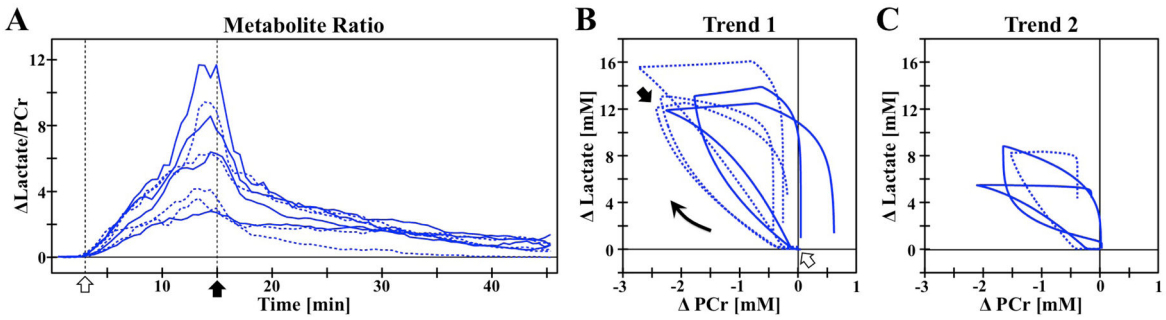

Figure 3.

(A) Temporal ratio of ΔLactate/[PCr] for individual rats for occlusion (open arrow) and reperfusion (closed arrow). Statistical comparison reveals two groups, whose dynamic correlation can be seen in the ΔLac versus ΔPCr plots for (A) Trend 1 and (B) Trend 2. The asymmetry of the correlation loop highlights the different temporal responses to occlusion versus reperfusion. First (solid) and second (dashed) occlusions indicated within each trend.

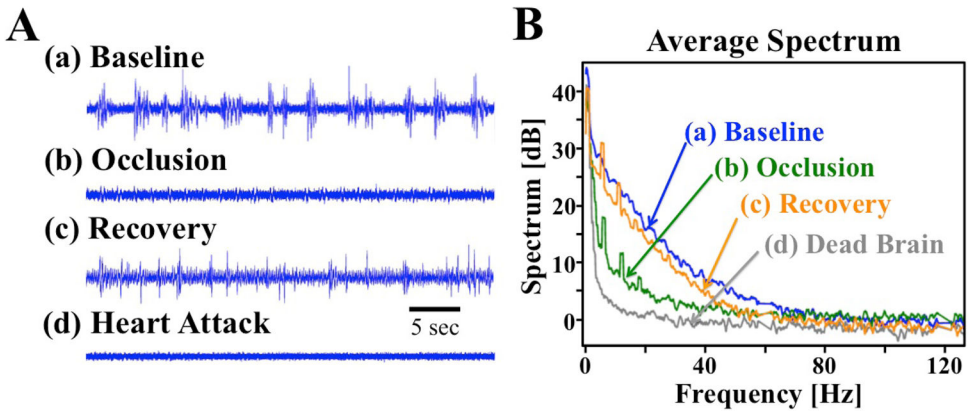

Figure 4.

(A) Filtered time course clips and (B) average power spectrum from (a) baseline, (b) 8 minutes following occlusion onset, (c) an hour after reperfusion, and (d) *ex vivo*. Power is calculated based on $10*log_{10}$ of the amplitude of the corresponding time-frequency spectrogram.

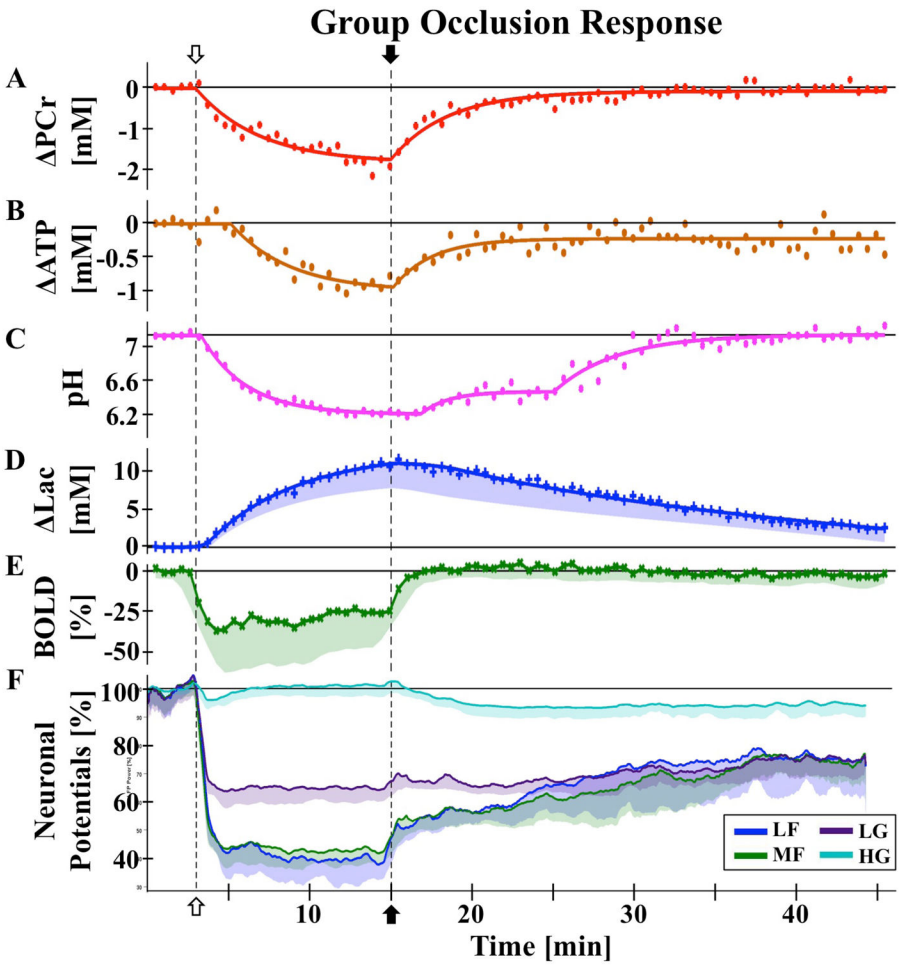

Figure 5.

Group responses to occlusion (open arrow) and reperfusion (closed arrow) with raw data (symbols) and regression fits (lines) for (A) ΔPCr, (B) ΔATP, (C) pH, and (D) ΔLac, raw data for (E) BOLD, and smoothed data (lines) for (F) neuronal field potential activity. (A–C) Values quantified from average ^{31}P spectrum. (D–F) Average of individual animal values, with shaded areas indicating one standard deviation (σ) from the mean. Field potentials were analyzed across 4 frequency bands: LF 0-10 Hz, MF 10-30 Hz, LG 30-58 Hz, and HG 62-200 Hz. Neither ATP nor field potential bands recover to baseline levels. Investigation of rat brain hemodynamic,